


## Gravitational drainage on a vertical substrate of a narrow width

Nan Xue  and Howard A. Stone \*

*Department of Mechanical and Aerospace Engineering, Princeton University,  
Princeton, New Jersey 08544, USA*

 (Received 13 September 2021; accepted 22 December 2021; published 6 January 2022)

The effect of a single, vertical edge on a draining liquid film was studied recently [*Phys. Rev. Lett.* **125**, 064502 (2020)]. In this experimental study, we characterize the structure of a liquid film, draining due to gravity, on a vertical, narrow substrate. We show that surface tension affects the draining film at the two vertical edges. The edge effects propagate into the film to eventually influence the shape over the entire width. Interferometry is performed to measure the film thickness profile. A motorized stage is used to vertically translate the thin film and the substrate, which extends the range of the measurements. Our experiments show that the thickness of the liquid film scales with the well-known Jeffreys' solution, which is the thickness of a draining film on a vertical substrate of infinite width. However, due to the existence of the two vertical edges, near the top contact line, the film thickness changes sharply near the edges and is flat near the middle of the substrate. In contrast, away from the top contact line, the edge effects propagate towards the middle, and the overall horizontal film shape eventually becomes approximately quartic. Further, we identify characteristic length scales in the vertical direction, which combine the effects of the surface tension, viscosity, and gravitational drainage. These length scales, respectively, highlight the effects from the vertical edges and the top contact line, and the experimental results are in agreement with the scaling arguments.

DOI: [10.1103/PhysRevFluids.7.014001](https://doi.org/10.1103/PhysRevFluids.7.014001)

### I. INTRODUCTION

A liquid film on a planar substrate naturally drains and flows under the action of gravity. Usually there are two typical modes of a gravitational flow that spreads on a substrate:

(1) Draining and spreading due to the variation of the film thickness. Examples are the gravitational spreading of a liquid on a horizontal surface, such as flooding by the breaking of a dam [1], industrial wastewater slumping into a river [2], and fluid injection into porous rocks [3].

(2) Draining and spreading due, at least in part, to the inclination of the substrate. Examples are the gravitational spreading of a liquid on a steep slope [4–6], and related situations such as chocolate coating on a sphere [7] and lava flows from a volcano [8]. In these scenarios, instabilities are usually observed associated with the effect of surface tension. For example, on an incline, the fingering instability occurs at the moving contact line of a spreading liquid film [9–12]. On the other hand, dripping, i.e., the Rayleigh-Taylor instability, occurs on a liquid film under an inclined plate [13–15]. These instabilities may guide pattern formations in soft materials [16].

From the perspective of modeling, for the case that viscous effects dominate inertial effects, the thickness profile  $h$  of a thin film on a planar substrate satisfies [17–20]

$$3\mu \frac{\partial h}{\partial t} = -\nabla \cdot [h^3 \nabla (\gamma \nabla^2 h)] + \nabla \cdot [h^3 \nabla (\rho g h \cos \alpha)] - 3\rho g h^2 \frac{\partial h}{\partial x} \sin \alpha, \quad (1)$$

\*hastone@princeton.edu

where  $\mu$  is the dynamic viscosity of the liquid,  $t$  is the time that the liquid drains,  $\gamma$  is the surface tension of the liquid,  $\rho$  is the density of the liquid,  $\alpha$  is the inclination angle of the substrate from the horizontal direction, and  $x$  is the position along the inclined substrate. The four terms in Eq. (1) are, respectively, the viscous, surface tension, and two gravitational drainage contributions. The two gravitational terms highlight the two modes of gravitational flows described above, respectively.

Certainly, both of the gravitational terms in Eq. (1) drive the drainage of a thin film for  $\alpha \neq 0$  and 90 degrees [5,19]. In this study, we are interested in a draining liquid film on a vertical substrate, i.e.,  $\alpha = 90$  degrees, and the substrate is of finite width. We focus on the film that is away from the bottom bath, where the film connects to a macroscopic meniscus [21,22]. Also, we consider no external influx into the film during the gravitational drainage. If we focus on the center of the film without the effects of the edges, then by balancing the viscous term and the gravitational term (the fourth term) in Eq. (1), the film thickness profile is

$$h_J(x, t) = \left( \frac{\mu x}{\rho g t} \right)^{1/2}, \quad (2)$$

where  $x$  is the vertical position of the liquid film and is in the direction of gravity. Equation (2) is Jeffreys' solution [23], which is a self-similar solution for the thickness profile of a draining film on a two-dimensional vertical plate, i.e., the plate is infinitely wide in the horizontal direction. Jeffreys' solution is robust and reproducible and has even been used to design a viscometer [24,25].

Jeffreys' solution predicts the film thickness profile in the limit of a wide substrate. However, as implied in Eq. (1), when the width of the film is relatively narrow, surface tension plays a role in the draining film where there is a variation of the film thickness in the horizontal direction. For example, a thin, slender rivulet on an inclined substrate drains under the action of gravity, and the horizontal shape of the rivulet is modified by surface tension [17,20]. The contact line of the rivulet moves during the drainage. From the perspective of modeling and according to our experience with the experiments, the moving contact line is associated with the wetting property, e.g., contact angle hysteresis, of the liquid on the substrate and thus is a complex question that is beyond the scope of this paper.

In contrast, the draining film on a vertical substrate near a vertical edge provides a simple geometry to quantify and validate the effect of surface tension on the film shape [26]. In this geometry, the contact line is pinned at the vertical edge. In our previous work, we showed that the film thickness profile near the vertical edge is self-similar in the limit that the substrate is wide and the surface tension only affects a local region near the edge. Based on Jeffreys' solution, a self-similar solution was constructed to analyze the thickness profile of the draining film near the edge (this solution was also indicated in Ref. [20]). Moreover, this self-similar solution converts three independent variables in the nonlinear partial differential equation into one independent variable for an ordinary differential equation, which is a unique feature of this problem and might inspire modeling in other systems.

The self-similar solution in our previous work predicts the thickness profile of a draining film near a vertical edge. However, in reality, there are always two edges on a vertical substrate. When the two edges are relatively close, i.e., the substrate is narrow, the overall thickness profile of the draining film might be affected by both of the edges, which, to the best of our knowledge, has not been studied. For example, it is not known what is the thin-film shape and even whether the thin-film thickness profile scales with Jeffreys' solution. Also, it is of practical interest, e.g., for coating, to provide a guideline on how wide a substrate needs to be to maintain a uniform coating thickness in the middle. This threshold of width is certainly a function of the vertical length of the substrate. In this article, we attempt to show experimentally the answers and further give some analysis to these questions.

In this work, we show the effects of surface tension when a thin liquid (silicone oil) film drains on a vertical, narrow substrate. Interferometry is performed to demonstrate and measure the thickness profile of the liquid film. The substrate is fixed on a motorized stage, which translates vertically and

enables scanning and the measurements of the liquid film thickness profile over an extended range of  $O(10^2)$  mm in the vertical direction. The setup is shown in Sec. II. The results of interferometry in Secs. III A and III B show that, as the vertical position increases in the flow direction, the boundary, where surface tension introduces an edge effect, propagates from the edge to the middle of the substrate: near the top contact line, the vertical edges affect the film only locally, and the film thickness profile near the middle of the substrate is horizontally uniform, following Jeffreys' solution, except for a small region, of several millimeters, at the top contact line where surface tension matters; away from the top contact line, the vertical edges affect the film shape over at least some of the horizontal direction. The horizontal film shape eventually becomes approximately quartic, but the thickness of the film at the centerline still scales with Jeffreys' solution. In detail, the film thickness profile at the apex of the approximately quartic shape is approximately 20% higher than Jeffreys' solution. Further, in Sec. III C a length scale is identified in the vertical direction, which compares and balances viscous, surface tension, and gravitational effects, in the region away from the top contact line. In Sec. III D another vertical length scale is proposed to characterize the edge effects localized near the top contact line. As part of our investigation, we change the viscosities of the silicone oils, the time that the thin film drains, and the widths of the glass substrates. As a result, in Sec. III E, we show that all the experimental results agree with our scaling arguments.

## II. EXPERIMENTAL SETUPS

To highlight the effect of the surface tension acting at the edges of the substrate, we used narrow glass substrates in the experiments. The substrates were usually several millimeters in width  $w$ , with length  $l = 114$  mm, so that  $w \ll l$ . The glass substrates were originally  $95 \times 114$  mm (Ted Pella Inc.) and were cut by a glass cutter to the desired width  $w$ . The resulting narrow substrates were approximately uniform in width. To confirm the uniformity of the substrates, we measured the width at the top ( $w_{\text{top}}$ ) and bottom ends ( $w_{\text{bot}}$ ) with calipers. The mean width was then calculated by  $w = (w_{\text{top}} + w_{\text{bot}})/2$  and was reported as the width of the glass substrate. In the experiments, the width of the substrate varied approximately from 2 to 50 mm. Typically the relative variation of the width  $|w_{\text{top}} - w_{\text{bot}}|/w < 5\%$ . A summary of all of the glass substrates used in the experiments and the corresponding measurements of the widths is given in Table I in Appendix A.

After cutting, the glass substrate was cleaned with isopropanol and then fixed vertically on a motorized stage. The substrate was carefully aligned within 0.5 degree in the direction of gravity. To create a viscous liquid film, a pipette was moved horizontally along the substrate and deposited the silicone oil (Sigma-Aldrich). Below the top horizontal contact line, the silicone oil spread over the substrate until it reached the two vertical edges. Five silicone oils, which are Newtonian fluids and completely wet the glass substrates, were used to achieve a range of viscosities for the experiments; the silicone oils used were the same as these used in our previous study [26]. The viscosities of the silicone oils in the experiments were, respectively,  $\mu = 20.8, 51.5, 102, 540, \text{ and } 1081$  mPa s, as measured with a rheometer (CP50-1, MCR 301, Anton Paar; the shear rate  $\dot{\gamma}$  ranged from 1 to  $100 \text{ s}^{-1}$ ). The surface tensions of the silicone oils were, correspondingly,  $\gamma = 21, 21, 21, 22, \text{ and } 22$  mN/m, and the densities were  $\rho = 0.95, 0.96, 0.96, 0.97, \text{ and } 0.97 \times 10^3 \text{ kg/m}^3$ , respectively. We note that the material properties of the silicone oils remained nearly constant for years. For example, the viscosities of the silicone oils changed less than 2% in 2 yr.

The thin liquid films drained on the glass substrate due to the action of gravity and were typically tens of micrometers in thickness. Interferometry was performed to visualize and measure the thickness profile of the thin film. A sketch of the interferometric setup is shown in Fig. 1(a), and a demonstration of the draining liquid film is provided in Fig. 1(b). A He-Ne laser (wavelength  $\lambda = 633$  nm, Thorlabs) illuminated the draining thin film, and the reflected rays were collected with a high-speed camera (Phantom v7.3). The collected rays in the camera were mainly reflected from the air-oil and glass-air interfaces, which create constructive and destructive interferometric patterns and indicate the thickness profile of the thin film. Figures 2(a)–2(d) show the typical

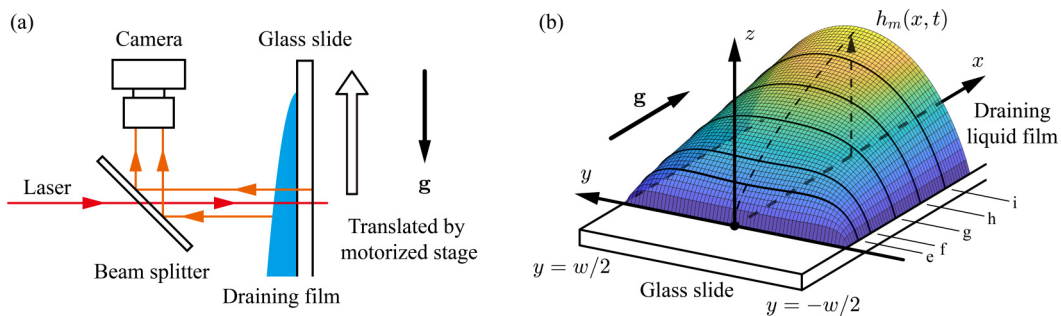


FIG. 1. Schematics of the experimental setup and a draining liquid film on a vertical glass substrate. (a) A sketch of the interferometric setup for measuring the thickness of the liquid film on a transparent substrate of width  $w$ . A pipette moved horizontally along the substrate and injected the silicone oil to create a draining liquid film. The beam from a He-Ne laser (wavelength  $\lambda = 633$  nm) passed through a beam splitter and illuminated the liquid film, and the reflected rays were collected with a high-speed camera. The reflected rays on the air-oil and glass-air interfaces created the constructive and destructive fringes in the interferometric pattern. A glass slide was fixed to a motorized stage, which translated upwards. Due to this translation, the interferometric patterns of the draining liquid film were captured along an extended range of vertical positions. (b) A schematic of the gravitationally draining liquid film on a glass slide of width  $w$ . This schematic is constructed from the ODE solution [Eq. (6) with the boundary conditions in Eq. (8)], which is an approximation to the shape of the draining film. The top contact line, where  $x = 0$ , is pinned throughout the experiment. The solid black lines at the interface of the liquid film labeled e–i, respectively, represent the film thickness profiles in the horizontal direction  $y$ , which are also displayed as the solid black lines in Figs. 2(e)–2(i). The thickness of the draining film along the centerline (dashed black line) of the substrate,  $h_m(x, t)$ , is the focus of the measurements in the experiments.

interferometric patterns produced in the experiments. The neighboring fringes, i.e., the black-to-black or white-to-white fringes, indicated a difference in the film thickness of  $\lambda/(2n)$ , where  $n = 1.4$  is the refractive index of the silicone oil. We note that the information of the thickness variation of the glass substrate was also included in the interferometric patterns, which was discussed in our previous studies [26,27]. Here the glass substrates were 0.19–0.25 mm thick. According to our interferometric imaging, the thickness variation of the glass substrates was much smaller than the thickness variation of the thin film. Also, the gradient of the thickness variation along the substrate was in the horizontal direction, i.e., the thickness of the substrates mostly varied in the horizontal direction and was uniform vertically. In this study we focus on the vertical film thickness profile along the centerline in the systematic measurements, and thus the variations associated with the thickness of the glass substrate were negligible.

Typically, the imaging and measurements with interferometry are restricted by the field of view of imaging, which is affected by the components of the optical setup, such as the lens and the size of the sensor and beam splitter. For example, in our setup, the field of view of high-speed imaging was 3.8 (width)  $\times$  2.9 (height) mm (800  $\times$  600 pixels). In the experiments, the thin film on the substrate translated upwards with the motorized stage. The interferometric patterns were recorded during the vertical translation. Therefore, we were able to construct the film thickness profile over an extended range of vertical positions by transferring the temporal imaging intensities, i.e., the interferometric patterns during the translation, as a function of time  $t$ , to the spatial film thickness profile, as a function of the vertical position  $x$ .

We started the vertical translation of the motorized stage at  $t_0$ , where  $t_0$  is the period from the end of the liquid deposition to the start of the translation. We denote  $t_0$  as the *initial time* throughout this article. Initially, the top contact line was right at the bottom of the field of view. At the initial time  $t_0$ , the motorized stage starts to translate upwards with a constant speed  $v = 1$  mm/s (calibrated),

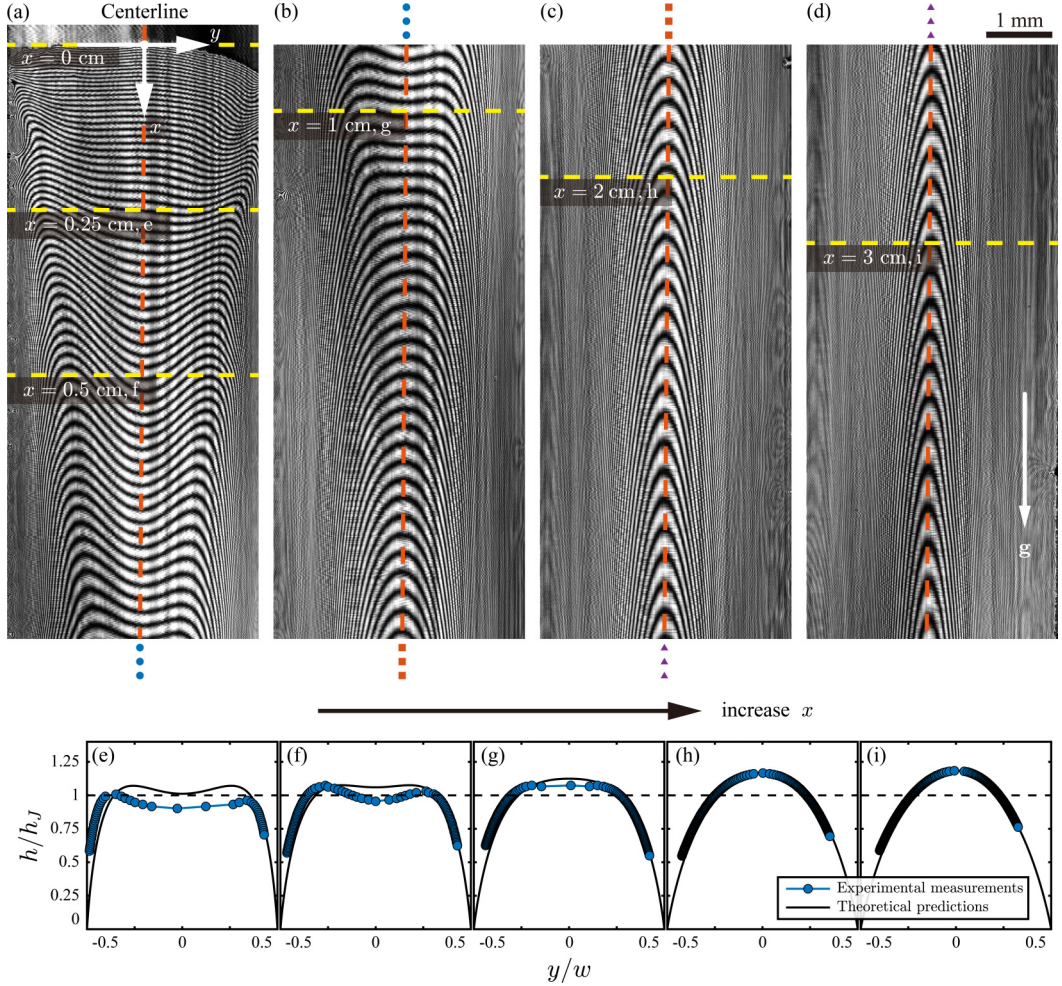


FIG. 2. Interferometric patterns and measurements of a draining liquid film. The viscosity of the liquid is  $\mu = 102$  mPa s, the initial time is  $t_0 = 8$  min, and the width of the glass slide is  $w = 4.03$  mm. (a)–(d) The interferometric patterns of the draining liquid film with ranges of the vertical position (a)  $x = 0-0.9$ , (b)  $0.9-1.8$ , (c)  $1.8-2.7$ , and (d)  $2.7-3.6$  cm, respectively. The dashed red lines represent the centerline of the liquid film where  $y = 0$ . (e)–(i) The horizontal thickness profile of the liquid film normalized by Jeffreys’ solution,  $h/h_J$ , as a function of the normalized horizontal position  $y/w$ , at the vertical positions (e)  $x = 0.25$ , (f)  $0.5$ , (g)  $1$ , (h)  $2$ , and (i)  $3$  cm. These vertical positions are also marked as horizontal dashed yellow lines in the interferometric patterns (a)–(d). The blue circles denote the film thickness profile measured by interferometry, and the solid black lines denote the model predictions based on the ODE (6) with the boundary conditions (8). At small vertical positions  $x$ , the experimental measurements slightly deviate from the model predictions. This difference is due to (1) the fact that the top contact line is not perfectly flat in the experiments and (2) the surface tension effect from the top contact line that will be discussed in Sec. III D but is not considered in the model here.

where the stage accelerated to this constant speed  $v$  within  $0.1$  s; the acceleration did not affect the draining of the thin film since the acceleration of the motorized stage was still much less than the gravitational acceleration. While the liquid film was translated upwards, interferometric image sequences were captured by the high-speed camera with a frame rate of 100 frames per second

(fps). To construct the interferometric patterns of the liquid film, we focus on recording the intensity profile on a fixed horizontal line in the field of view. Specifically, this horizontal line was 25 pixels higher than the bottom line of the field of view; see the gray line in Supplemental Movie 1 [28]. While the liquid film was translating upwards, the horizontal line was scanned vertically through the draining film. In the data processing, the temporal intensity profile on the line as a function of time  $t$  was converted to the spatial interferometric patterns of the thin film as a function of the vertical position  $x$ . The vertical position  $x$  was linear with the time  $t$  since the speed of the translation  $v$  was constant.

Typical interferometric patterns recorded using the above procedures are shown in Figs. 2(a)–2(d) and 6(a)–6(d) (in Appendix B); Supplemental Movie 1 [28] is an example of the recorded field of view while the motorized stage translated upwards. With this translation, we were able to capture the features of the draining film on the glass substrates over an extended range in the vertical direction, e.g., up to  $O(10^2)$  mm in our setup, compared to 3 mm, which is the height of the field of view. We note that the film drained continuously during the vertical translation, and the interferometric patterns produced throughout the vertical scanning indicated the film thickness profile  $h(x, y, t)$ , which is then presented and compared with Jeffreys’ solution  $h_J(x, t)$  in Sec. III.

### III. EXPERIMENTAL RESULTS AND DISCUSSIONS

In Secs. III A and III B, we focus on experimentally estimating the thickness profile of the draining liquid film on a narrow, vertical substrate in the horizontal and vertical directions, respectively. In Secs. III C and III D, we focus on modeling the surface tension effects on the draining film from the vertical edges and top contact line, respectively. Finally, in Sec. III E we present the experimental results by spanning a large parameter space and show the agreement between our measurements and scaling arguments.

#### A. Horizontal thickness profile of the draining film

A schematic of the thin film configuration is shown in Fig. 1(b). The liquid film rests on a vertical glass slide of width  $w$ . The top contact line of the liquid film is horizontal and is pinned throughout the experiment. We denote  $x$  as the vertical position in the direction of gravity, while  $x = 0$  is the position of the top contact line. Also, we denote  $y$  as the horizontal position, where  $y = 0$  represents the vertical centerline of the liquid film and  $y = \pm w/2$  represent the two vertical edges of a substrate. In this section we document the horizontal thickness profile of the liquid film at a constant  $x$ , e.g., the solid black lines at the interface of the liquid film in Fig. 1(b).

Typical interferometric patterns of a draining thin film on a vertical, narrow glass slide are presented in Figs. 2(a)–2(d); see the movie of the field of view during the vertical translation in Supplemental Movie 1 [28]. The two vertical edges of the glass slide are approximately at the left and right sides of the image. The interferometric patterns show the variation of the horizontal thickness profile of the liquid film as the vertical position  $x$  increases. Near the top contact line [Fig. 2(a),  $x = 0$  to 0.25 cm], the interferometric fringes near the middle are mostly straight horizontal lines, which indicates that the liquid film is uniform horizontally away from the vertical edges and the film thickness increases with  $x$ . Away from the top contact line (increasing  $x$ ), the fringes are no longer straight horizontal lines, which indicates that the film thickness near the middle of the liquid film varies horizontally, because of surface tension, as a consequence of the existence of the two vertical edges; the thickness of the film changes rapidly near the edges. Over much of the film, the fringes are dense and approximately vertical near the vertical edges, which indicates that the gradient of the film thickness is large and primarily in the horizontal direction. With increasing  $x$ , the vertical fringes are observed to be denser, and the region of the vertical fringes expands towards the centerline of the thin film, which also indicates that the influence of the two edges is more significant at large vertical positions.

To further analyze the structure of the liquid film, the interferometric patterns are processed to determine the film thickness profile. The film thickness  $h = 0$  at the top contact line. The absolute film thickness profile is constructed by processing the interferometric patterns from the contact line, e.g., counting the number of fringes. The constructed thickness profile  $h$  in the horizontal direction (as a function of  $y$ ) for different vertical positions  $x$  is shown in Figs. 2(e)–2(i). The thickness profile is normalized by Jeffreys’ solution [Eq. (2)], which is the thickness of the draining film on a vertical plate with infinite width (at the same time  $t$  and the same vertical position  $x$  as the measurement). We observe that the gradient of the film thickness is large near the edges. Close to the top contact line, the horizontal thickness profile shows two peaks [Fig. 2(e)]. From the edge to the centerline of the film, the thickness increases and then decreases to Jeffreys’ solution  $h_J$ , which is very similar to the feature of the draining film near a single, vertical edge, reported in our previous study [26]. The measurement shows that for small  $x$ , the effect from the other edge is negligible. In contrast, away from the top contact line, the two peaks merge in the middle, and the thickness profile has a plateau-like shape [Fig. 2(f)]. For further increasing  $x$ , the plateau-like shape narrows [Fig. 2(g)], and then the thickness profile becomes approximately quartic [Figs. 2(g) and 2(h)]. At large vertical position  $x$ , the thickness profile remains approximately quartic until the motorized stage reaches the end and stops; see Fig. 6 in Appendix B. In Appendix C we discuss the quartic function that can approximate the film shape.

Away from the top contact line, the horizontal thin film shape transits from a plateau-like shape with two visible peaks [Fig. 2(e)] to an approximately quartic shape [Fig. 2(i)]. This change of the shapes along the direction of drainage highlights the propagation of the boundary of the edge-affected region towards the centerline. The transition of the film shape as a function of the vertical position  $x$  also brings to mind capillary leveling of a rectangular trench in a viscous film as a function of time [29], though the governing equations are different.

### B. Vertical thickness profile of the draining film

The horizontal film thickness profile is complex but symmetric about the centerline; e.g., see the vertical dashed red lines marked in Figs. 2(a)–2(d). The thickness at the centerline of the liquid film,  $h_m(x, t)$ , is a significant parameter that describes the structure of the draining film with the two vertical edges. We denote  $h_m$  as the *film center thickness*. In Secs. III B and III E, we focus on the measurements and discussion of  $h_m$ .

Interferometric patterns are processed to construct the film thickness profile at the centerline of the film,  $h_m(x, t)$ . In particular,  $h_m = 0$  at the top contact line ( $x = 0$ ), and  $h_m(x, t)$  during the vertical translation is measured by counting the interferometric fringes. The vertical translation,  $v = 1$  mm/s, starts at the initial time  $t = t_0$ , when the field of view is at the top contact line,  $x = 0$ . Thus, when the field of view is at  $x$ , the local drainage time  $t = x/v + t_0$ . Therefore, our measurement of the draining film during the vertical translation indicates  $h_m(x, t) = h_m(x, x/v + t_0)$ .

A typical measurement of  $h_m(x, t)$  is presented as the blue circles in Fig. 3(a). Indeed,  $h_m$  increases with the vertical position  $x$ . To compare with  $h_m$ , we use Jeffreys’ solution  $h_J$  [Eq. (2)], the thickness of a draining film where there is no edge effect, i.e., the plate is infinitely wide; see the dashed line in Fig. 3(a). Note that to compare with the measurements by interferometry, Jeffreys’ solution  $h_J(x, t)$  in Fig. 3(a) is presented with the same drainage time  $t$  and vertical position  $x$  as  $h_m(x, t)$ . In particular,  $h_J(x, t = x/v + t_0) = [\frac{\mu x}{\rho g(x/v + t_0)}]^{1/2}$ . As a result of the comparison, near the top contact line, the film center thickness is close to Jeffreys’ solution [Fig. 3(a),  $x \lesssim 1$  cm]. However, away from the top contact line, the film center thickness  $h_m$  deviates from and is larger than the prediction based on Jeffreys’ solution [Fig. 3(a),  $x \gtrsim 1$  cm]. This deviation is due to the surface tension effects from the vertical edges: while  $x$  increases, the boundary of the edge-affected region propagates towards the centerline. The horizontal film shape transits from a flat plateau-like shape to an approximately quartic shape [the insets in Fig. 3(b)], and the measurements of  $h_m$  deviate from Jeffreys’ solution. In Sec. III C we will focus on analyzing the vertical length scale that describes the propagation of the edge effects towards the centerline.

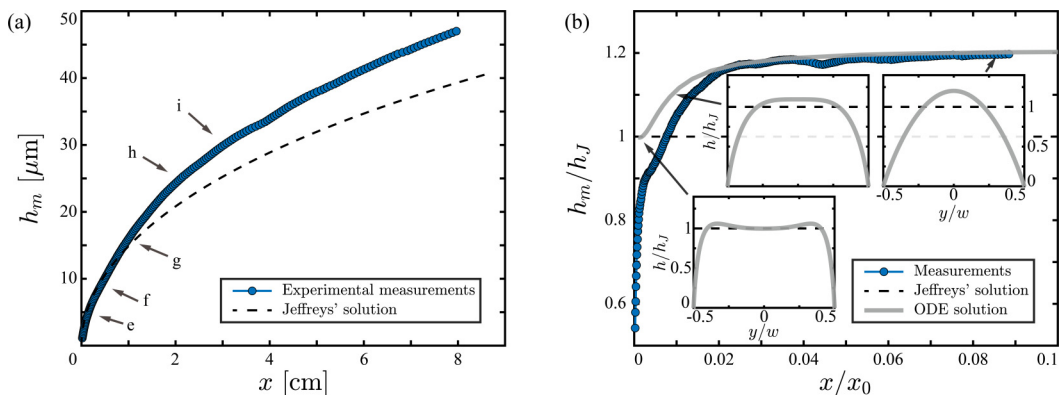


FIG. 3. The film thickness profile at the centerline of the liquid film. The experiment is the same as displayed in Fig. 2. (a) The film thickness at the centerline,  $h_m$ , as a function of the vertical position  $x$ . The markers labeled e–i denote the vertical positions where the film shapes are displayed in Figs. 2(e)–2(i). (b) The film thickness at the centerline normalized by Jeffrey’s solution,  $h_m/h_J$ , as a function of the normalized vertical position  $x/x_0$ , where  $x_0$  is the vertical length scale that describes the surface tension effects, given by Eq. (7). The solid blue lines with circles, the dashed lines, and the solid gray lines represent, respectively, the interferometric measurements, Jeffrey’s solution, and the prediction based on the ODE solution [Eq. (6) with the boundary conditions in Eq. (8)]. The insets in (b) show the horizontal film thickness profile,  $h/h_J$  as a function of  $y/w$ , according to the solution of the ODE (6) with the boundary conditions in Eq. (8).

### C. Modeling and approximation by the self-similarity scaling argument

In this section we focus on developing a scaling argument for the draining liquid film on a vertical substrate of width  $w$ . The schematic of the model is shown in Fig. 1(b). We start with standard thin-film analysis. We are interested in the regime where the vertical edges affect the thickness profile of the thin film. In this regime, the gradient of the film thickness profile is mostly in the horizontal direction, i.e.,  $|\partial/\partial y| \gg |\partial/\partial x|$ . The thickness profile of the liquid film  $h(x, y, t)$  satisfies [17–20,26]

$$3\mu \frac{\partial h}{\partial t} = -\gamma \frac{\partial}{\partial y} \left( h^3 \frac{\partial^3 h}{\partial y^3} \right) - 3\rho g h^2 \frac{\partial h}{\partial x}. \quad (3)$$

The three terms in Eq. (3) are, respectively, the viscous, surface tension, and gravitational drainage contributions. We note that we are interested in the late-time behavior of the liquid film, when the effect of the initial film thickness profile is negligible [11]. In our previous study [26] (also suggested in Ref. [20]), a similarity solution was proposed based on Jeffrey’s solution, so that (in this case  $y = 0$  denotes the single vertical edge)

$$h(x, y, t) = h_J(x, t)F(\eta) = (\mu x / \rho g t)^{1/2} F(\eta), \quad (4)$$

where

$$\eta = \frac{(\rho g)^{3/8} t^{1/8} y}{\gamma^{1/4} \mu^{1/8} x^{3/8}}. \quad (5)$$

The exponents in Eq. (5) are fixed by the three terms in the partial differential equation (PDE) (3), and the form of the self-similar solution in Eq. (4) utilizes the assumption that the film is described by Jeffrey’s solution far from the edge. Boundary conditions accounting for the finite width of the geometry would typically be expected to disallow a simple similarity solution. However, we will show in this article that, though the boundary conditions are not perfectly satisfied, the self-similar solution still provides a reasonable approximation that agrees with our experiments.



Substituting Eqs. (4) and (5) into Eq. (3), the PDE becomes an ordinary differential equation (ODE) with the form [20,26]

$$-F + \frac{1}{4}\eta F' + \frac{2}{3}(F^3 F''')' + F^3 - \frac{3}{4}\eta F^2 F' = 0. \quad (6)$$

The similarity variable given by Eq. (5) converts the three independent variables, i.e., the vertical position  $x$ , the horizontal position  $y$ , and the time that the film drains  $t$ , into a single variable  $\eta$ . The PDE with three independent variables [Eq. (3)] is also converted to an ODE [Eq. (6)]. Equation (5) balances the surface tension, viscous, and gravitational drainage terms, and characterizes the scale of the boundary-layer region where the liquid film is affected by the vertical edges. We note again that Eq. (6) does not guarantee an exact solution of the film thickness profile since the boundary conditions of the geometry also need to specifically satisfy the self-similarity by Eq. (5), i.e., the boundary conditions of  $\eta$  need to be independent of  $x$ ,  $y$ , and  $t$ . In this article, in the geometry of a vertical substrate of a narrow width, the scaling argument represented by Eq. (5) will be used to analyze the propagation of the boundary of the edge-affected region towards the centerline.

In our previous work [26], we analyzed the surface tension effects on a draining film near a single, vertical edge. In this scenario, the position of the vertical edge was denoted as  $y = 0$  and the other edge of the substrate was far away. In such a geometry,  $\eta$  as scaled in Eq. (5) can be interpreted as a dimensionless scale in the horizontal direction. A small value of  $\eta$  (e.g.,  $\eta \lesssim 1$ ) indicates that the position is close to the edge, and the film thickness profile varies sharply in the horizontal direction. In contrast, a large value of  $\eta$  (e.g.,  $\eta \gtrsim 5$ ) represents a position far away from the edge, and the film thickness profile is uniform horizontally. A given value of  $\eta$  specifies the boundary of the region where the film thickness is affected by the vertical edges.

In this article, we consider the draining film on a vertical, narrow substrate, and the distance between the two vertical edges is  $w$ . To make an approximate argument for the propagation of the edge effect from one vertical edge to the other, we set the horizontal position to be  $y = w$  in Eq. (5). Also we set  $\eta = 1$  in Eq. (5) as the threshold for the boundary of the edge-affected region. According to Eq. (5), we get a vertical length scale  $x_0$  that

$$x_0 = \frac{\rho g t^{1/3} w^{8/3}}{\gamma^{2/3} \mu^{1/3}}. \quad (7)$$

Equation (7) combines the effects of surface tension, viscosity, and gravitational drainage in one variable  $x_0$ , which is an alternative vertical length scale that describes the propagation of the edge effects due to surface tension towards the centerline. Note that  $y = w$  and  $\eta = 1$  is selected so that there is no prefactor in Eq. (7). A further discussion of other selections of  $y$  and  $\eta$  can be found in Sec. III E. The estimate given by Eq. (7) is our main deduction and will be used to display and compare our experimental results, e.g., in Figs. 3(b) and 5(b) and Figs. S2(b), S3(b), and S4(b) in the Supplemental Material [28].

Besides the scaling argument of Eq. (7), it is also possible to make an approximate estimate of the film thickness profile,  $h(x, y, t)$ , based on the ODE in Eq. (6). We now consider the coordinates as shown in Fig. 1(b), where  $y = 0$  denotes the centerline of the liquid film, and the boundary conditions for our problem are  $h = 0$  at  $y = \pm w/2$ , i.e., the film thickness is zero at the two vertical edges. The other two boundary conditions could be, e.g., the contact angles at the two edges. Our previous work showed that setting the contact angle at the edge to zero gives a reasonable estimate of the film thickness profile [26]. A different selection of the contact property would lead to a minor difference in the thickness profile of the macroscopic film. For the symmetry of the configuration we also set  $\partial h / \partial y = 0$  at  $y = \pm w/2$ . The corresponding boundary conditions for the ODE [Eq. (6)] are

$$F = 0 \quad \text{and} \quad F' = 0, \quad \text{at} \quad \eta = \pm \eta_0, \quad (8)$$

where  $\eta_0 = \frac{1}{2} \frac{(\rho g)^{3/8} t^{1/8} w}{\gamma^{1/4} \mu^{1/8} x_0^{3/8}} = \frac{1}{2} \left(\frac{x}{x_0}\right)^{-3/8}$  and represents the dimensionless position of the two edges; Eq. (8) satisfies the symmetry condition at  $y = 0 = \eta$ .

We note that the dimensionless position of the boundary  $\eta_0$  is a function of  $x$  and  $t$  and is not a constant. Therefore, given the boundary conditions in our problem, the ODE [Eq. (6)] and the corresponding boundary conditions [Eq. (8)] do not provide an exact self-similar solution for the film thickness profile  $h(x, y, t)$ , since the nonconstant boundary conditions violate the self-similarity as a horizontal length scale  $w$  is introduced into the problem. However, the solution of the ODE [Eq. (6)] with the boundary conditions [Eq. (8)] potentially provides an approximate estimate of the structure of the liquid film and will be used to compare with our experimental results, e.g., in Figs. 3(b) and 5(b) and Figs. S2(b), S3(b), and S4(b) [28]. Solving the thin-film equation is not the focus of this article, but fully solving the PDE [Eq. (3)] numerically and the examination of the film thickness profile near the vertical edges could be interesting topics for future investigations.

We use the MATLAB BVP (boundary value problems) solver `bvp5c` to solve the ODE [Eq. (6)]. Similar to our previous work [26], we set the boundary conditions as  $F(\pm\eta_0) = 10^{-4}$  to avoid singularities at the edges and  $F'(\pm\eta_0) = 0$ . As a detail of the setup of the numerical solver, we restrict the maximum number of mesh points to be less than  $2 \times 10^5$  and the relative error to be less than  $10^{-6}$ . We input an initial guess solution to start the numerical solving as  $F = F' = F'' = F''' = 1$  in the interval  $[-\eta_0, \eta_0]$ . We change the value of  $\eta_0$  to get different structures of the film thickness [note that  $F(\eta) \equiv h/h_J$ ], to compare with the experimental measurements at different vertical positions  $x$ .

Typical results of the ODE solution [Eq. (6)] are displayed as the solid black lines in Figs. 2(e)–2(i) and 6(e)–6(i) (in Appendix B). The numerical solution agrees with our experimental measurements of the horizontal film thickness profile. Near the top contact line,  $x/x_0$  is small so that  $\eta_0$  is large. A large value of  $\eta_0$  indicates that the liquid film near the middle is away from the surface tension effects from the edges. The film thickness profile resembles a plateau-like shape with two visible peaks [Fig. 2(e)]. In contrast, away from the top contact line,  $x/x_0$  is large so that  $\eta_0$  is small. A small value of  $\eta_0$  indicates that the liquid film is affected by the existence of the vertical edges. The film thickness profile remains an approximately quartic shape for large  $x/x_0$  [Figs. 6(e)–6(i)]. It is interesting to note that though the use of similarity solution in this article introduces an inconsistency of the applied boundary conditions [Eq. (8)], the similarity approximation still agrees with the experimental measurements. This bears some resemblance to the use of a similarity solution for cornered drops, where the boundary conditions are not perfectly satisfied but can be complemented with the boundary-layer-like structure near the contact line [30,31].

To compare with our experimental measurements of the film thickness profile at the vertical centerline  $h_m$ , we solve the ODE [Eq. (6)] and calculate the film thickness at the center, where  $\eta = 0$  [note that  $F(0) = h_m/h_J$ ], with different input values of  $\eta_0$  [note that  $\eta_0 = \frac{1}{2}(x/x_0)^{-3/8}$ ]. We then display the normalized film center thickness,  $h_m/h_J$ , as a function of the normalized vertical position,  $x/x_0$ , together with our experimental results; see the solid gray lines in Fig. 3(b).  $h_m/h_J$  is the ratio of the center film thickness to the prediction based on Jeffreys' solution, which is the film thickness where there is no effect from the edges, e.g., the vertical substrate is infinitely wide. This ratio  $h_m/h_J$  highlights the surface tension effects from the edges.  $h_m/h_J$  increases away from the top contact line, as  $x/x_0$  increases. The ratio then remains approximately constant,  $h_m/h_J \approx 1.2$ , for  $x/x_0 \gtrsim 0.05$ , while the horizontal thickness profile of the liquid film remains approximately quartic. However, close to the top contact line,  $h_m/h_J$  is observed to be less than unity and is due to the surface tension effect from the top contact line. This edge effect from the top contact line will be discussed next in Sec. III D.

### D. Measurement of the film thickness near the top contact line

To analyze the edge effect from the top contact line of the draining film, we performed experiments on wide glass substrates. The width of the substrates is  $w \approx 47.5$  mm. The corresponding vertical length scale where the film center thickness is affected by the vertical edges is  $x_0 = O(10^4)$  mm. Therefore, near the middle of the wide substrates the film shapes are not affected by the vertical edges. We changed the viscosities of the silicone oils  $\mu$  from 20.8 to 1081 mPa s,

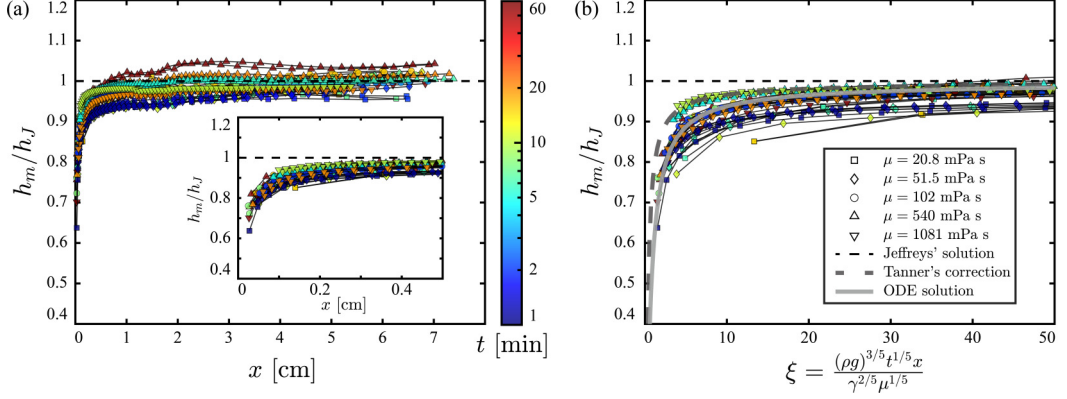


FIG. 4. The normalized film thickness profile at the centerline of the liquid film,  $h_m/h_J$ , while the substrates are wide ( $w = 47.5$  mm). The viscosities of the liquid are  $\mu = 20.8$  (squares), 51.5 (diamonds), 102 (circles), 540 (upward-pointing triangles), and 1081 (downward-pointing triangles) mPa s, respectively. The color bar indicates the drainage time  $t$  (note the logarithmic scale). (a)  $h_m/h_J$  as a function of the vertical position  $x$ . The inset is a close-up view of  $h_m/h_J$  near the top contact line (where  $x \leq 0.5$  cm and is small). (b)  $h_m/h_J$  as a function of the dimensionless vertical position  $\xi$ , which represents the edge effect caused by the top contact line. The dashed black line, the dashed gray line, and the solid gray line, respectively, represent Jeffreys' solution [Eq. (2)], Tanner's correction [Eq. (13)], and the ODE solution [Eq. (12)]. For the best presentation of the result, the density of the data is diluted, i.e., the number of the data points on each line presented is reduced by a factor of five. A full display of the data set is provided in Fig. S1 [28].

and the initial time  $t_0$  (when the vertical translation starts) from 1 to 60 min; see the list of the experiments performed in Table I below.

Figure 4 shows the film center thickness measurements,  $h_m(x, t)$ , on vertical, wide substrates. To compare with Jeffreys' solution  $h_J$ , we take the ratio  $h_m/h_J$  and display this ratio as a function of the vertical position  $x$ ; see Fig. 4(a). Away from the top contact line (e.g.,  $x \gtrsim 2$  cm), the film center thickness  $h_m$  is close to the prediction given by Jeffreys' solution  $h_J$ . We note that the ratio  $h_m/h_J$  at large  $x$  is not identical to unity due to the experimental errors such as the vertical variation of the thickness of the substrate (the result is sensitive to the noise in the experiments since we take the ratio of experimental signals). In contrast, near the top contact line [e.g.,  $x \lesssim 0.2$  cm in the inset of Fig. 4(a)], the film center thickness  $h_m$  deviates from Jeffreys' solution. The ratio  $h_m/h_J$  decreases significantly when approaching the top contact line,  $x = 0$ . This deviation is due to the edge effect from the top contact line.

We perform standard thin-film analysis to estimate the surface tension effect from the top contact line. For simplicity, we consider the liquid film that is uniform in the horizontal direction, i.e., the substrate is infinitely wide and the gradient on the film is only in the vertical direction. In this scenario, we denote the thickness profile of the liquid film as  $h_c(x, t)$ , to distinguish it from the film thickness  $h(x, y, t)$  where there is an effect from the vertical edges. Note that in our experiments,  $h_m(x, t)$  approaches  $h_c(x, t)$  when the width  $w$  is sufficiently large. Simplifying starting with Eq. (1),  $h_c(x, t)$  satisfies (an alternative, but similar approach, is given in Ref. [25])

$$3\mu \frac{\partial h_c}{\partial t} = -\gamma \frac{\partial}{\partial x} \left( h_c^3 \frac{\partial^3 h_c}{\partial x^3} \right) - 3\rho g h_c^2 \frac{\partial h_c}{\partial x}. \quad (9)$$

The three terms in Eq. (9) are the viscous, surface tension, and gravitational drainage effects, respectively. We consider the late-time behavior of the liquid film, and the effect of the initial film thickness profile is negligible. The structure of the three terms enables a similarity solution,

$$h_c(x, t) = At^{-3/5} G(Bxt^{1/5}) = At^{-3/5} G(\xi), \quad (10)$$

where  $\xi = Bxt^{1/5}$  is an independent dimensionless similarity variable that describes the edge effect from the top contact line. Substituting Eq. (10) into Eq. (9), we find  $A = \frac{\gamma^{1/5}\mu^{3/5}}{(\rho g)^{4/5}}$ , and  $B = \frac{(\rho g)^{3/5}}{\gamma^{2/5}\mu^{1/5}}$ . Correspondingly,

$$\xi = \frac{(\rho g)^{3/5}t^{1/5}x}{\gamma^{2/5}\mu^{1/5}}. \quad (11)$$

The PDE that describes the film thickness profile [Eq. (9)] becomes an ODE,

$$-\frac{9}{5}G + \frac{3}{5}\xi G' + (G^3 G''')' + 3G^2 G' = 0. \quad (12)$$

It is interesting to note that Eq. (12) is the same as the ODE that describes the thin film in the arrested bubble problem, while the boundary conditions are different [32]. For the boundary conditions here, we note that the film thickness profile is Jeffreys' solution away from the top contact line. The corresponding boundary conditions for  $G(\xi)$  is  $G(\xi) \rightarrow \xi^{1/2}$  at  $\xi \rightarrow \infty$ , which counts as two boundary conditions (equations for  $G$  and  $G'$ , respectively) at infinity. The third boundary condition is  $G = 0$  at  $\xi = 0$ , i.e., the film thickness is zero at the top contact line. The fourth boundary condition is the contact angle at the top contact line, and we choose  $G' = 0$  at  $\xi = 0$  since silicone oil completely wets the glass substrate. With these four boundary conditions, we can solve the ODE in Eq. (11) to achieve the film thickness profile  $h_c(x, t)$ .

We use the MATLAB BVP solver `bvp5c` to solve Eq. (11). In particular, we solve for  $G(\xi)$  in the interval  $\xi \in [0, \xi_0]$ , where  $\xi_0$  is the right boundary of the domain and is selected as  $\xi_0 = 100$  for demonstration. Note that changing  $\xi_0$  will change slightly the numerical results, but the features of the solutions are similar. The boundary conditions for the numerics are, respectively,  $G(0) = 0.01$  (to avoid the singularity at the contact line),  $G'(0) = 0$ ,  $G(\xi_0) = \xi_0^{1/2}$ , and  $G'(\xi_0) = \frac{1}{2}\xi_0^{-1/2}$ . We restrict the maximum number of mesh points to be less than  $5 \times 10^4$  and the relative error to be less than  $10^{-6}$ . The initial guess solution is  $G(\xi) = \xi^{1/2}$  in the interval  $[0, \xi_0]$ . As a detail of the numerics, we note that projecting the interval  $[0, \xi_0]$  to  $[0, 1]$  (by setting  $\xi^* = \xi/\xi_0$ ) will stabilize the numerical solving, but the ODE in Eq. (12) and the corresponding boundary conditions need to be rescaled by  $\xi^*$  accordingly.

The numerical solution of Eq. (12) is shown as the solid gray line in Fig. 4(b). In the experiments, the width of the substrate  $w$  is sufficiently large so that our measurement of the film thickness in the middle  $h_m(x, t)$  indicates  $h_c(x, t)$ . Therefore, we merge the notations  $h_m(x, t)$  and  $h_c(x, t)$  in the comparison with the experiments. In particular, we present the ratio of the film thickness to the prediction by Jeffreys' solution,  $h_m/h_J$ , as a function of the independent self-similar variable  $\xi$ , which describes the edge effect by the top contact line. We note that Tanner also proposed a correction to the film thickness profile near the top contact line [25], which can be expressed in our notations as

$$(h_m/h_J)^2 + k \frac{(h_m/h_J)^{1/3}}{\xi^{5/6}} = 1, \quad (13)$$

where  $k \approx 0.455$  is a constant that is calculated by the numerical computation in Ref. [25]. Tanner's correction is derived mainly using an asymptotic approach and is displayed as the dashed gray line in Fig. 4(b). As a result, both Tanner's correction and our solution of the ODE (12) predict the deviation of the film thickness profile from Jeffreys' solution, near the top contact line. Our ODE solution is slightly closer to the experimental measurements since it is directly the similarity solution of the thin-film equation [Eq. (9)]. Further, we note that Figs. 4(a) and 4(b) are similar due to the fact that the power of  $t$  is much smaller than the power of  $x$  in the expression of  $\xi$ . The spread of the measured  $h_m/h_J$  at small  $\xi$  is due to experimental error, such as the top contact line is not perfectly horizontal, though the differences are negligible away from the top contact line.

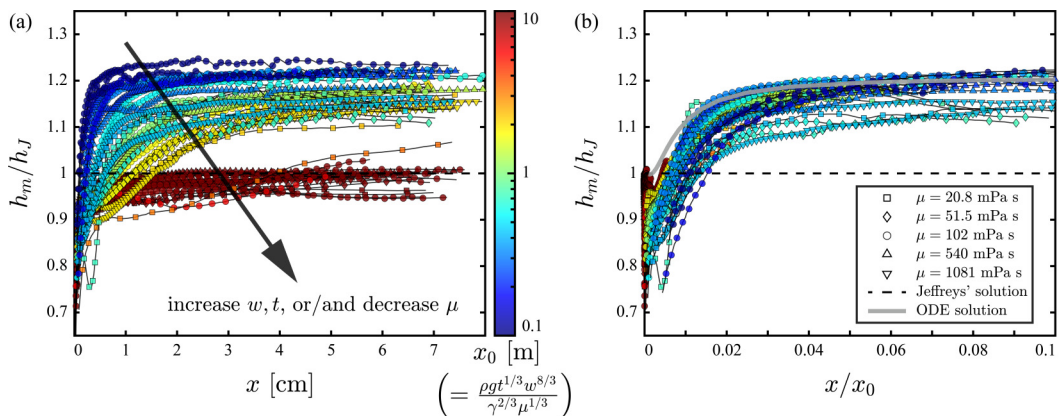


FIG. 5. The normalized film thickness profile at the centerline of the liquid film,  $h_m/h_J$ . The width of the substrate  $w$  varies from 2 to 47.5 mm. The viscosities of the liquid are  $\mu = 20.8$  (squares), 51.5 (diamonds), 102 (circles), 540 (upward-pointing triangles), and 1081 (downward-pointing triangles) mPa s, respectively. The color bar indicates the vertical length scale  $x_0$  by Eq. (7) (note the logarithmic scale). (a)  $h_m/h_J$  as a function of the vertical position  $x$ . (b)  $h_m/h_J$  as a function of the normalized vertical position  $x/x_0$ . The dashed black line represents Jeffreys' solution, and the solid gray line represents the ODE solution (6) with the boundary conditions Eq. (8). For the best presentation of the result, only a portion of the data is displayed, i.e., only the result of the experiments with the shortest initial time  $t_0$  in each trial is displayed; see the description in Table I below. Also, the number of the data points on each line presented is reduced by a factor of five. A full display of the data set is in Fig. S4 [28].

### E. Measurement of the film thickness at the centerline

In this section we focus on demonstrating the thickness profile of the liquid film along the vertical centerline with the effect of the vertical edges. To achieve a large parameter space in the experiments, we use different silicone oils to tune the viscosities  $\mu$  from 20.8 to 1081 mPa s. The initial time  $t_0$  (when the vertical translation starts) varies from 40 to 3720 s. The widths of the prepared glass substrates vary from 1.97 to 47.5 mm. A list of experiments performed is displayed in Table I below. We measured the film center thickness profile  $h_m$  as a function of the vertical position  $x$ . To compare with our modeling, we normalize  $h_m$  with Jeffreys' solution  $h_J$ , which is the film thickness profile where there are no surface tension effects from the vertical edges.

The results of the experiments are displayed in Fig. 5. Certainly, the measured  $h_m(x, t)$  varies significantly with different  $\mu$ ,  $t$ , and  $w$  [Fig. 5(a)]. A decrease in the width of the substrate  $w$  leads to an enhancement in the edge effects to the middle: the transition of the horizontal film thickness profile from a plateau-like shape to an approximately quartic shape occurs at a smaller vertical position, and the ratio  $h_m/h_J$  rapidly increases to approximately 1.2, where the film shape becomes approximately quartic. On the other hand, a decrease in the viscosity  $\mu$  or an increase in the time  $t$  leads to thinner films and therefore a reduction in the surface tension effects associated with the edges. The control experiments with different  $w$  or different  $\mu$  are presented in Figs. S2 and S3 [28], respectively. All the experimental data are presented in Fig. S4 [28].

The scaling law (7) shows a vertical length scale that quantifies the edge effects to the middle of the liquid film.  $x_0$  combines the effects of the surface tension, viscosity, and gravitational drainage, increases with  $w$  or  $t$ , and decreases with  $\mu$ . Larger values of  $x_0$  indicate weaker edge effects, and the film thickness profile remains close to Jeffreys' solution for longer vertical distance before it becomes approximately quartic; see the shift from the blue data points to the red data points in Fig. 5(a). Note that the red data points in Fig. 5(a) are similar to Jeffreys' solution since the width  $w$  is large, but we expect these ratios  $h_m/h_J$  to rise to approximately 1.2 where  $x$  is sufficiently long (e.g., one meter).

Though the ratio  $h_m/h_J$  as a function of  $x$  spreads significantly with different  $w$ ,  $t$ , and  $\mu$ , by normalizing the vertical position  $x$  by the vertical length scale  $x_0$  [Eq. (7)], the results approximately collapse and agree with the approximation based on the ODE solution [Eq. (6) with the boundary conditions in Eq. (8)]; see Fig. 5(b). The upper limit of  $x$  is approximately 8 cm in the experiments, and thus, the results with large  $x_0$  are in the region of small  $x/x_0$  in Fig. 5(b). For example, the red data points [ $x_0 = O(10)$  m] are in the region where  $x/x_0 \lesssim 0.01$  in Fig. 5(b). We note that the data do not tightly collapse to a single curve due to the experimental errors, such as (1) the edge effect from the top contact line, which is discussed in Sec. III D, (2) the variation of the substrate thickness in the vertical direction, and (3) the nonuniformity of the contact, or wetting, properties at the vertical edges. Slight local dewetting might occur at the edges.

As  $x/x_0$  increases, the horizontal film shape transits from a plateau-like shape to an approximately quartic shape, and the ratio  $h_m/h_J$  increases to approximately 1.2. The film shape remains approximately quartic for  $x/x_0 \gtrsim 0.05$ . Inspired by Ref. [20], an estimate of the shape of the steady approximately quartic shape is made in Appendix C. On the other hand, we note that the draining film is a thin film throughout the experiments, i.e.,  $h \ll w$ . However, when the narrow substrate is sufficiently long, e.g.,  $x = O(10)$  m,  $h$  increases with the vertical distance and approaches  $w$ , the thin-film analysis breaks down, and we expect the ratio  $h_m/h_J$  to decrease to less than unity.

Finally, we note that the transition of the film shape is expected to occur at  $x/x_0 \approx 0.02$  [e.g., Fig. 5(b)], which is much less than unity. This small value of  $x/x_0$  is due to the selection of the scales in our scaling argument [Eq. (7)]. In practice, if we select  $y = w/2$ , which is the distance between the vertical edge and the center, and  $\eta = 2$ , where we reported in our previous work [26] that the film shape reaches a peak at  $\eta \approx 2$ , the scaling of the vertical length becomes

$$x_0^* = \frac{1}{2^{16/3}} \frac{\rho g t^{1/3} w^{8/3}}{\gamma^{2/3} \mu^{1/3}} = \frac{x_0}{2^{16/3}} \approx \frac{x_0}{40} \approx 0.02x_0. \quad (14)$$

The length scale  $x_0^*$  is a more practical presentation of the length scale that describes the vertical edge effects on the liquid film for drainage on a vertical, narrow substrate. The middle of the liquid film is affected by the edges, and the horizontal film thickness profile becomes approximately quartic where  $x/x_0^* \gtrsim 1$ .

#### IV. CONCLUSIONS

In this article, we characterized the thickness profile of a draining film on a vertical, narrow substrate. Silicone oils with different viscosities and glass substrates with different widths were used in the experiments. A motorized stage was used to translate the liquid film on the glass substrate vertically, and the thickness profile of the draining film was measured with interferometry, over an extended range [ $O(10^2)$  mm] in the vertical direction. The interferometric measurements indicated that, away from the top contact line, the overall film thickness profile is affected from the edges by surface tension. As the vertical position  $x$  increases, the film thickness profile in the horizontal direction transits from a plateau-like shape with two visible peaks to an approximately quartic shape, and the structure of the approximately quartic shape remains constant for large  $x$ . Though affected by the vertical edges, the thickness of the liquid film still scales with Jeffreys' solution. Away from the top contact line, the ratio of the film center thickness  $h_m$  to the prediction of Jeffreys' solution increases to approximately 1.2 and then remains approximately constant. Further, scaling arguments were made to analyze (1) the propagation of the region where surface tension is important, from the vertical edges to the centerline of the liquid film and (2) the surface tension effect on the liquid film near the top contact line. Vertical length scales which respectively represent the edge effects from the vertical edges and the top contact line were proposed and demonstrated. As a result, we find good agreements between the experimental measurements and our scaling arguments. Looking forward, the construction of a numerical simulation to fully solve the thin-film equation to examine the asymptotic limit of the self-similar approximation and the analysis of the contact, or wetting, properties at the edges remain topics for future investigations.

### ACKNOWLEDGMENTS

The authors thank Jens Eggers for reading the original manuscript and constructive discussions. The authors thank the anonymous referees for their valuable suggestions for improvement of the original manuscript. N.X. acknowledges Princeton University through a Charlotte Elizabeth Procter Fellowship.

### APPENDIX A: CONDITIONS OF THE EXPERIMENTS

Table I displays all of the experimental conditions presented in this study. The table respectively displays the series (no.) of the glass substrate, the measured width of the top end of the substrate  $w_{\text{top}}$ , the measured width of the bottom end of the substrate  $w_{\text{bot}}$ , the mean width of the glass substrate  $w [(w_{\text{top}} + w_{\text{bot}})/2]$ , the viscosity of the liquid  $\mu$ , the series of the trial, i.e., the number of times that the silicone oil was injected on the same glass substrate, and the initial time  $t_0$  when the experiment starts and the glass substrate starts to translate upwards.

### APPENDIX B: INTERFEROMETRIC PATTERNS OF THE DRAINING FILM (EXTENDED)

Figure 6 shows the interferometric patterns and the measurements of the draining film over an extended vertical position. Figure 6 is an extended version of Fig. 2. The vertical positions are  $x = 3.6\text{--}8.4$  cm. For large values of the vertical position  $x$ , the interferometric patterns are similar to each other, and the film thickness profile in the horizontal direction remains approximately quartic.

### APPENDIX C: THE APPROXIMATELY QUARTIC SHAPE OF THE DRAINING FILM

Here we attempt to model the steady approximately quartic shape of the draining film in the horizontal direction, at large  $x/x_0$ . We start from the standard thin-film equation [Eq. (3)]. We seek the solution of the film thickness profile,  $h(x, y, t)$ , based on Jeffreys' solution. The film thickness profile is

$$h(x, y, t) = h_f(x, t)H(x, y, t) = (\mu x / \rho g t)^{1/2} H(x, y, t). \quad (\text{C1})$$

Substituting Eq. (C1) into Eq. (3), we get that

$$-\frac{3}{2}H + 3t \frac{\partial H}{\partial t} = -\frac{\gamma \mu^{1/2} x^{3/2}}{(\rho g)^{3/2} t^{1/2}} \frac{\partial}{\partial y} \left( H^3 \frac{\partial^3 H}{\partial y^3} \right) - 3H^2 \left( \frac{1}{2}H + x \frac{\partial H}{\partial x} \right). \quad (\text{C2})$$

In our experimental observations, away from the top contact line, the film thickness profile in the horizontal direction remains the same as an approximately quartic shape, i.e.,  $H$  does not change with  $x$  or  $t$ . This observation indicates that the terms  $\partial H / \partial x$  and  $\partial H / \partial t$  are negligible. Also, we set  $Y = y/w$  for simpler presentations. Equation (C2) then becomes

$$-H + H^3 + \frac{2}{3} \frac{\gamma \mu^{1/2} x^{3/2}}{(\rho g)^{3/2} t^{1/2} w^4} \frac{\partial}{\partial Y} \left( H^3 \frac{\partial^3 H}{\partial Y^3} \right) = 0. \quad (\text{C3})$$

We are interested in the film thickness structure  $H$  in the horizontal direction,  $H(Y)$ . To estimate  $H(Y)$ , we collect the terms of  $H(Y)$  in the Taylor's series near  $Y = 0$ ; note that  $H(Y)$  is an even function. In particular, we set  $H(y)$  to be quartic,

$$H(y) = a - bY^2 - cY^4, \quad (\text{C4})$$

where  $a, b, c$  are constants, which can be a function of  $x$  or  $t$  but are independent on  $Y$ . The boundary conditions are  $H = 0$  at  $Y = \pm \frac{1}{2}$ , i.e., the film thickness is zero at the edges, where  $y = \pm \frac{1}{2}w$ . We do not yet set the contact properties at the edges due to the fact that we have only three degrees of freedom ( $a, b$ , and  $c$ ) in the expansion. Also, for simplicity of the expression, we denote that

TABLE I. The conditions of the experiments. The experiments with substrates no. 6, 9, 22, 26, and 29 are processed to construct Figs. 4 and S1 [28]. The experiments with substrates no. 1–29 (only with the initial time  $t_0$  set in boldface) are processed to construct Fig. 5. The experiments with substrates no. 10–22 are processed to construct Fig. S2 [28]. The experiments with substrates no. 1–5, 7, 8, 14, 16, 23–25, 27, and 28 are processed to construct Fig. S3 [28]. All the results from the experiments are used to construct Fig. S4 [28].

Substrate no.	$w_{\text{top}}$ [mm]	$w_{\text{bot}}$ [mm]	$w$ [mm]	$\mu$ [mPa s]	Trial no.	$t_0$ [s]
1	3.24	3.36	3.30	20.8	1	<b>45</b>
2	3.82	3.92	3.87	20.8	1	<b>60</b>
					2	<b>60</b>
3	4.14	4.28	4.21	20.8	1	<b>40</b>
4	5.70	5.88	5.79	20.8	1	<b>60</b>
5	5.76	5.84	5.80	20.8	1	<b>40; 300; 600; 1200</b>
					2	<b>300; 600</b>
6	~47.5	~47.5	~47.5	20.8	1	<b>60; 360; 900</b>
					2	<b>60; 360; 900</b>
7	4.06	4.06	4.06	51.5	1	<b>90</b>
					2	<b>60</b>
8	6.10	6.12	6.11	51.5	1	<b>62</b>
					2	<b>61</b>
9	~47.5	~47.5	~47.5	51.5	1	<b>64; 361</b>
					2	<b>60; 362; 662</b>
10	1.94	2.00	1.97	102	1	<b>120; 480; 900</b>
					2	<b>120; 480; 900</b>
11	2.26	2.30	2.28	102	1	<b>120; 480; 900</b>
12	2.54	2.48	2.51	102	1	<b>125</b>
13	3.22	3.38	3.30	102	1	<b>120; 480; 900</b>
					2	<b>120; 480; 900</b>
14	4.04	4.02	4.03	102	1	<b>120; 480; 900</b>
					2	<b>120; 480; 900</b>
15	5.12	5.12	5.12	102	1	<b>120; 480; 900</b>
					2	<b>120; 480; 900</b>
16	6.08	6.26	6.17	102	1	<b>120; 480; 900</b>
					2	<b>128; 480; 900</b>
17	8.36	8.66	8.51	102	1	<b>480; 900</b>
18	11.46	11.88	11.67	102	1	<b>120; 480; 900</b>
19	14.98	14.90	14.94	102	1	<b>120; 480; 900</b>
					2	<b>120; 480; 900</b>
20	20.44	20.18	20.31	102	1	<b>162; 480; 900</b>
					2	<b>120; 480; 900</b>
21	30.30	31.00	30.65	102	1	<b>120; 480; 900</b>
					2	<b>120; 480; 900</b>
22	~47.5	~47.5	~47.5	102	1	<b>120; 480; 900</b>
					2	<b>120; 480; 900</b>
23	3.16	3.24	3.20	540	1	<b>300; 1200</b>
					2	<b>300; 1800; 3720</b>
24	3.60	3.54	3.57	540	1	<b>360</b>
25	6.04	6.08	6.06	540	1	<b>300; 1200; 3600</b>
					2	<b>300; 1200; 3630</b>
26	~47.5	~47.5	~47.5	540	1	<b>300; 1200; 3600</b>
					2	<b>300; 1200; 3720</b>
27	4.10	4.18	4.14	1081	1	<b>600; 1200; 3600</b>
					2	<b>632; 1200; 3600</b>
28	7.16	7.16	7.16	1081	1	<b>610; 1200; 3600</b>
					2	<b>600; 1220; 3600</b>
29	~47.5	~47.5	~47.5	1081	1	<b>600; 1200; 3600</b>
					2	<b>600; 1200; 3610</b>



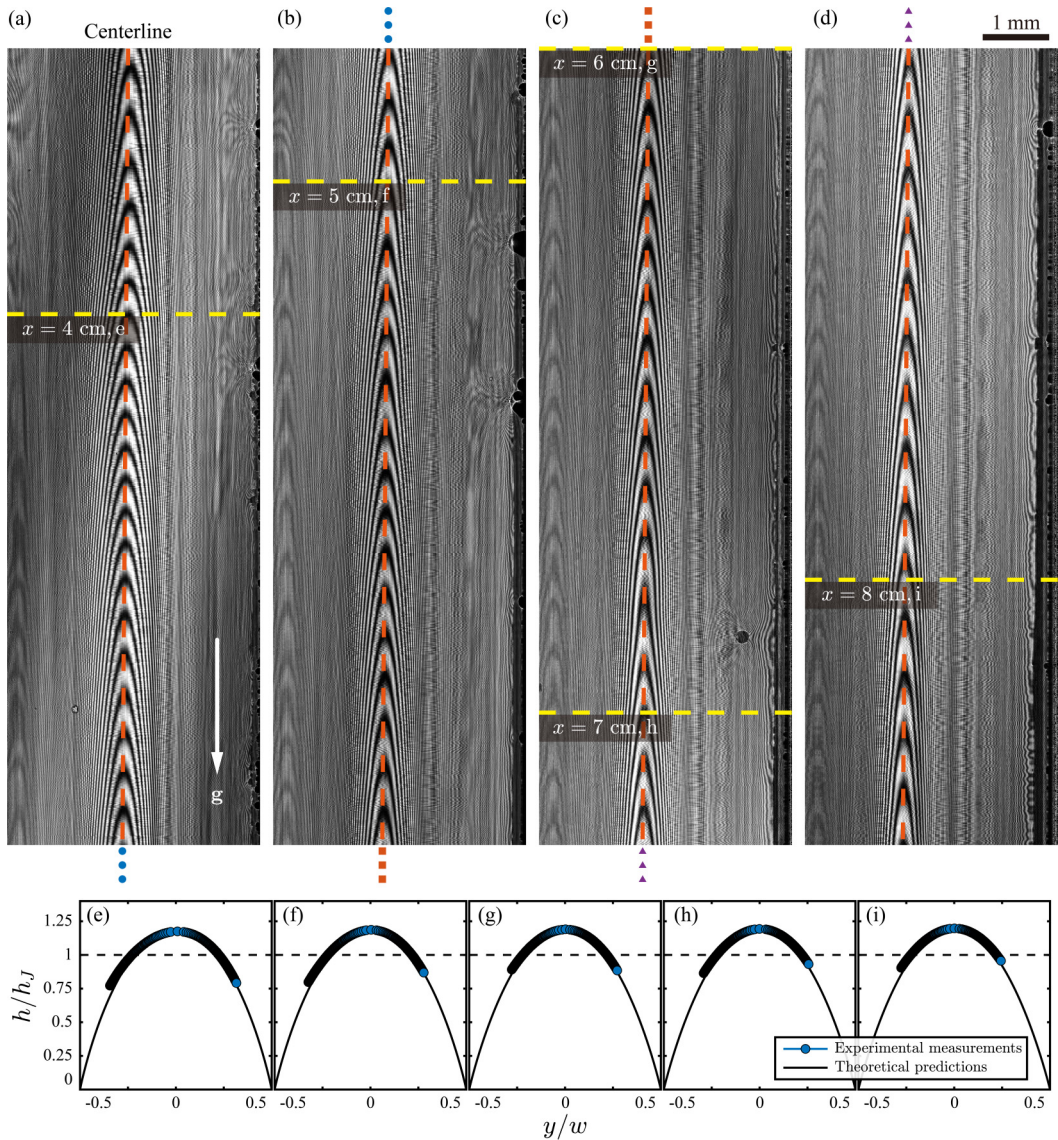


FIG. 6. Interferometric patterns and measurements of the draining liquid film. This figure is an extended version of Fig. 2, and the vertical positions are  $x = 3.6\text{--}8.4$  cm. The viscosity of the liquid is  $\mu = 102$  mPa s, the initial time is  $t_0 = 8$  min, and the width of the glass slide is  $w = 4.03$  mm. (a)–(d) The interferometric patterns of the draining liquid film with ranges of the vertical position (a)  $x = 3.6\text{--}4.8$ , (b)  $4.8\text{--}6$ , (c)  $6\text{--}7.2$ , and (d)  $7.2\text{--}8.4$  cm, respectively. The dashed red lines represent the centerline of the liquid film where  $y = 0$ . (e)–(i) The normalized horizontal thickness profile of the liquid film,  $h/h_J$ , as a function of the normalized horizontal position  $y/w$ , at the vertical positions (e)  $x = 4$ , (f) 5, (g) 6, (h) 7, and (i) 8 cm. These vertical positions are also marked as the horizontal dashed yellow lines in the interferometric patterns (a)–(d). The blue circles denote the film thickness profile measured by interferometry, and the solid black lines denote the model predictions based on the ODE (6) with the boundary conditions (8).

$K = \frac{\gamma\mu^{1/2}x^{3/2}}{(\rho g)^{3/2}l^{1/2}w^2} = \left(\frac{x}{x_0}\right)^{3/2}$ . Substituting Eq. (C4) in Eq. (C2), we can collect the leading-order terms that

$$y^0 : -a + a^3 - 16Ka^3c = 0, \quad (\text{C5a})$$

$$y^2 : b - 3a^2b + 144Ka^2bc = 0. \quad (\text{C5b})$$

The boundary condition indicates that

$$a - \frac{1}{4}b - \frac{1}{16}c = 0. \quad (\text{C6})$$

As a result, the solution of Eqs. (C5) and (C6) is

$$a = \frac{2}{\sqrt{3}}, \quad (\text{C7a})$$

$$b = \frac{2048\sqrt{3}K - 3}{768K}, \quad (\text{C7b})$$

$$c = \frac{1}{64K}. \quad (\text{C7c})$$

Equations (C4) and (C7) give an estimate of the horizontal quartic profile of the liquid film thickness, away from the top contact line. We note that  $H(0) = a = 2/\sqrt{3} \approx 1.155$  and is similar to the observation in the experiments that  $h_m/h_J \approx 1.2$  for large  $x/x_0$  (note that  $H \equiv h_m/h_J$ ).

- 
- [1] M. Ungarish, *Gravity Currents and Intrusions: Analysis and Prediction* (World Scientific, Singapore, 2020), Vol. 1.
- [2] H. E. Huppert and J. E. Simpson, The slumping of gravity currents, *J. Fluid Mech.* **99**, 785 (1980).
- [3] Z. Zheng, B. Guo, I. C. Christov, M. A. Celia, and H. A. Stone, Flow regimes for fluid injection into a confined porous medium, *J. Fluid Mech.* **767**, 881 (2015).
- [4] P. C. Smith, A similarity solution for slow viscous flow down an inclined plane, *J. Fluid Mech.* **58**, 275 (1973).
- [5] J. R. Lister, Viscous flows down an inclined plane from point and line sources, *J. Fluid Mech.* **242**, 631 (1992).
- [6] F. J. Higuera, Steady creeping flow down a slope, *Phys. Fluids* **7**, 2918 (1995).
- [7] A. Lee, P.-T. Brun, J. Marthelot, G. Balestra, F. Gallaire, and P. M. Reis, Fabrication of slender elastic shells by the coating of curved surfaces, *Nat. Commun.* **7**, 11155 (2016).
- [8] R. W. Griffiths and J. H. Fink, Effects of surface cooling on the spreading of lava flows and domes, *J. Fluid Mech.* **252**, 667 (1993).
- [9] H. E. Huppert, Flow and instability of a viscous current down a slope, *Nature (London)* **300**, 427 (1982).
- [10] D. Takagi and H. E. Huppert, Flow and instability of thin films on a cylinder and sphere, *J. Fluid Mech.* **647**, 221 (2010).
- [11] N. Xue and H. A. Stone, Draining and spreading along geometries that cause converging flows: Viscous gravity currents on a downward-pointing cone and a bowl-shaped hemisphere, *Phys. Rev. Fluids* **6**, 043801 (2021).
- [12] T.-S. Lin, J. A. Dijkstra, and L. Kondic, Thin liquid films in a funnel, *J. Fluid Mech.* **924**, A26 (2021).
- [13] P. H. Trinh, H. Kim, N. Hammoud, P. D. Howell, S. J. Chapman, and H. A. Stone, Curvature suppresses the Rayleigh-Taylor instability, *Phys. Fluids* **26**, 051704 (2014).

- [14] A. Charogiannis, F. Denner, B. G. M. van Wachem, S. Kalliadasis, B. Scheid, and C. N. Markides, Experimental investigations of liquid falling films flowing under an inclined planar substrate, *Phys. Rev. Fluids* **3**, 114002 (2018).
- [15] P. G. Ledda and F. Gallaire, Secondary instability in thin film flows under an inclined plane: Growth of lenses on spatially developing rivulets, *Proc. R. Soc. A* **477**, 20210291 (2021).
- [16] E. Jambon-Puillet, M. R. Piéchaud, and P.-T. Brun, Elastic amplification of the Rayleigh–Taylor instability in solidifying melts, *Proc. Natl. Acad. Sci. USA* **118**, e2020701118 (2021).
- [17] B. R. Duffy and H. K. Moffatt, A similarity solution for viscous source flow on a vertical plane, *Eur. J. Appl. Math.* **8**, 37 (1997).
- [18] S. K. Wilson, B. R. Duffy, and S. H. Davis, On a slender dry patch in a liquid film draining under gravity down an inclined plane, *Eur. J. Appl. Math.* **12**, 233 (2001).
- [19] Y. M. Yatim, B. R. Duffy, S. K. Wilson, and R. Hunt, Similarity solutions for unsteady gravity-driven slender rivulets, *Q. J. Mech. Appl. Math.* **64**, 455 (2011).
- [20] N. A. Redwan and Y. M. Yatim, Unsteady flow of thin slender rivulets of a Newtonian fluid with strong surface-tension effect, in *AIP Conference Proceedings*, Vol. 2184 (AIP Publishing, New York, 2019), p. 060005.
- [21] L. Landau and B. Levich, Dragging of a liquid by a moving plate, *Acta Physicochim. URSS* **17**, 42 (1942).
- [22] M. Maleki, M. Reyssat, F. Restagno, D. Quéré, and C. Clanet, Landau–Levich menisci, *J. Colloid Interface Sci.* **354**, 359 (2011).
- [23] H. Jeffreys, The draining of a vertical plate, *Proc. Camb. Philos. Soc.* **26**, 204 (1930).
- [24] L. H. Tanner, The measurement of viscosity by optical techniques applied to a falling liquid film, *J. Phys. E: Sci. Instr.* **9**, 967 (1976).
- [25] L. H. Tanner, The surface tension effect on the flow of liquid down vertical or inclined surfaces, *J. Phys. D: Appl. Phys.* **13**, 1633 (1980).
- [26] N. Xue and H. A. Stone, Self-Similar Draining Near a Vertical Edge, *Phys. Rev. Lett.* **125**, 064502 (2020).
- [27] N. Xue, M. Y. Pack, and H. A. Stone, Marangoni-driven film climbing on a draining pre-wetted film, *J. Fluid Mech.* **886**, A24 (2020).
- [28] See Supplemental Material at <http://link.aps.org/supplemental/10.1103/PhysRevFluids.7.014001> for the movie and more experimental measurements.
- [29] O. Bäümchen, M. Benzaquen, T. Salez, J. D. McGraw, M. Backholm, P. Fowler, E. Raphaël, and K. Dalnoki-Veress, Relaxation and intermediate asymptotics of a rectangular trench in a viscous film, *Phys. Rev. E* **88**, 035001 (2013).
- [30] L. Limat and H. A. Stone, Three-dimensional lubrication model of a contact line corner singularity, *Europhys. Lett.* **65**, 365 (2004).
- [31] J. H. Snoeijer, N. Le Grand-Piteira, L. Limat, H. A. Stone, and J. Eggers, Cornered drops and rivulets, *Phys. Fluids* **19**, 042104 (2007).
- [32] C. Lamstaes and J. Eggers, Arrested bubble rise in a narrow tube, *J. Stat. Phys.* **167**, 656 (2017).